Low Resolution Spectroscopy of Miras 2—R Octantis

Bill Rea
6A Bygrave Place, Bishopdale, Christchurch 8053, New Zealand; rea.william@gmail.com

John C. Martin
Henry R. Barber Observatory, University of Illinois at Springfield

Received July 13, 2020; revised November 20, 30, 2020; accepted December 9, 2020

Abstract Low resolution spectroscopy with a filter wheel grating (R ~ 50–200) is an effective tool to monitor Mira type variables around their cycle. In early type Mira variables changes in spectral type are reflected in the depth of TiO absorption bands relative to nearby quasi-continuum points. However, those indices lose sensitivity in spectral types later/cooler than M6 or M7. Flux ratios between quasi-continuum points are better suited to monitor a cooler Mira like R Oct at low spectral resolution through its entire cycle. We identify flux ratios between quasi-continuum points in low resolution spectra that are sensitive enough to distinguish between comparison stars of different spectral types and find cycle-to-cycle differences in the behavior of R Oct around peak brightness. Those ratios are also much more sensitive than TiO to changes from mid to minimum in the cycle even when rendered less effective by lower signal to noise levels when R Oct approached minimum brightness.

1. Introduction

The long periods and large amplitudes of Mira variables make them a favorite observing target of non-professional observers using both visual and CCD photometry (Mattei1997). Those qualities also make them ideal targets for low resolution spectroscopy using filter wheel gratings spectrographs. As Wing (1997) notes: "If we think of Miras as variable stars with time-dependent spectra, it is clearly desirable to record both their spectroscopic and photometric behavior." While much of the professional focus on Mira variables has shifted to the infrared part of the spectrum, non-professionals limited by the sensitivity of silicon based CCD detectors, continue to observe mostly in the visual part of the spectrum. Readily available, low cost, filter-wheel gratings have made it easy to add routine low resolution spectroscopy to any CCD photometric observing program and the AAVSO Spectroscopic Database archives spectra of this type. Previous papers (Martin *et al.* 2016a, b; Rea 2019) addressed many issues relating both to the collection and interpretation of low resolution spectra of Miras through the use of filter wheel gratings, including problems associated with differential spectroscopy. The resolution of the spectra are very low with typical $R = \lambda / \Delta\lambda$ values from 50–200. However, even spectral resolutions this low record scientifically relevant changes in Mira variables.

The surface temperature of Mira variables change significantly over their pulsation cycle. As they fade in brightness their surface temperature cools, causing a shift in blackbody emission to longer wavelengths. Ideally that change could be measured from the peak and/or slope of the continuum flux relative to wavelength. However, in late type stars like Mira variables, strong molecular absorption features obliterate the continuum, particularly when recorded at low spectral resolution. So the presence and strength of key absorption features (mostly molecular bands) which also depend on temperature are the most reliable basis for determining temperature through spectral type (Gray and Corbally 2009). Wing (1992) proposed a narrow band photometric system to measure the spectral type for M-stars using the relative flux measured between points in the spectrum occupied by TiO molecular absorption bands and adjacent quasi-continuum. Azizi and Mirtorabi (2015) proposed refinements to that system intended for use with professional high resolution NIR spectroscopy.

The Wing ratio measures the strength of TiO absorption near 719 nm relative to quasi-continuum near 754 nm. Our investigation of the Mira variable X Oct (Rea 2019) used spectral peaks and troughs in the low resolution spectra to reproduce the diagnostic ratios for Mira variables in the Wing (1992) and Azizi and Mirtorabi (2015) systems. That work revealed as the star approached minimum brightness (its coolest temperature, about spectral type M7 for X Oct) the Wing ratio became unreliable due to interference by increasing VO molecular absorption. Azizi and Mirtorabi (2015) used a point at 704 nm to measure the continuum instead. But in the low resolution spectra of X Oct, the Azizi ratio was *less* sensitive to change in spectral type than the Wing ratio. While the Azizi ratio can work for high resolution IR spectra, that study showed it is not well suited for application with low resolution spectra.

Kirkpatrick *et al.* (1991) identified six points in M-type spectra between 630 and 900 nm that at sufficiently high spectral resolution measures the continuum free from molecular absorption (Table 1). Particularly at low spectral resolution, C2 (704 nm) corresponds to the Azizi and Mirtorabi (2015) continuum measurement and C3 (756 nm) corresponds to the Wing (1992) continuum measurement Wing B (754 nm).

Table 1. The six possible continuum points in spectral class K5 to M9 identified by Kirkpatrick *et al.* (1991).

Point	*Wavelength*
C1	653 nm
C2	704 nm
C3	756 nm
C4	813 nm
C5	884 nm
C6	904 nm

Given the 11-nm bandpass of the Wing B filter the small difference in central wavelength is not significant. At high spectral resolution, patches of continuum are clearly present around those points across most of the M-type spectral range. However, the low resolution of grating spectra only allow measurement quasi-continuum points affected by both continuum and nearby absorption.

Lower spectral resolution "blurs" the continuum with nearby absorption features. At the resolution of spectra obtained in this study one pixel on the CCD detector corresponds to more than 1 nm = 10 Å in wavelength. A single resolution unit in the spectrum (determined mostly by seeing profile in a slit-less spectrum) is several times that. The effect of absorption features on a given quasi-continuum point measured at low resolution can also change with spectral type. So at low spectral resolution each of these quasi-continuum points should be sensitive to changes in effective temperature over a fixed range of spectral types.

In this work we use the Pickles (1998) spectral library to predict the continuum points which can be used in ratios to measure the change in spectral type for stars later than M6. To test the predictions, we will focus on R Oct, which varies in spectral type from M5.3 to M8.4.

The remainder of this paper is structured as follows: section 2 describes the observing equipment, target stars, and methods; section 3 predicts which ratios of continuum points which should be most sensitive to changes in spectral type and effective temperature of Miras. Section 4 presents observations of R Oct and comparison stars, section 5 discusses how our observations of R Oct match the expectations, and section 6 explains our conclusions along with recommendations for implementing this method and direction of future work.

2. Observing equipment and methods

2.1. Observing equipment

Two telescopes were used in this study.

1. Rea operated an 80-mm f/6 Explore Scientific apochromatic refractor in Christchurch, New Zealand, with an Atik 414E Mono CCD camera using a SONY ICX424AL front-illuminated chip. The plate scale in the imaging plane was 2.77 arcseconds / pixel. Rea used a Paton Hawksley Star Analyzer 100 grating yielding a first order spectrum with a dispersion of 1.488 nm / pixel.

2. BSM_South of the AAVSOnet's Bright Star Monitors (https://www.aavso.org/bsm and https://www.aavso.org/bright-star-monitor-section). It was an AstroTech-72ED, a 72-mm, f/6 apochromatic refractor, located at Ellinbank Observatory in Victoria, Australia. At the time the data in this paper were collected it was fitted with an SBIG ST8-XME CCD camera and the filter wheel holding Astrodon high-thoughput Johnson and Cousins filters. The Johnson B, V, and I filters were used in this study.

2.2. Stars observed

Six stars were observed in this study. Basic details as well as results from this paper (discussed later) are presented in Table 2.

R Oct is a Mira variable close to the south celestial pole. The literature on R Oct is somewhat sparse owing to the difficulty of getting long-term grants of time on professional telescopes to monitor long period variables. The AAVSO International Database (AID) contains more than 6,000 visual observations of R Oct going back to 1893 (Kafka 2020). A VSTAR (Benn 2012) analysis of all the AAVSO visual photometry finds only one statistically significant period at 405.5 days photometric. A complementary analysis of a subset of the 2207 most recent visual observations using FAMIAS (Zima 2008) measures a 407-day period. Both are in good agreement with the 405- to 405.5-day periods found in the analysis of more sparsely sampled photometry by Celis (1978), deLaverny *et al.* (1997) and Serkowski and Shawl (2001).

Celis (1978), deLaverny *et al.* (1997) and Serkowski and Shawl (2001) classify R Oct as M5.5. Keenan (1966) reports spectral classification as M5.5e. Only deLaverny *et al.* (1997) gives a range: M5.3-M8.4.

2.3. Calibration and measurement of spectra

The spectra obtained with the gratings were extracted with SAOImage DS9 (https://sites.google.com/a/uis.edu/grating-spectroscopy-workshop/simple-spectrum-extraction-tutorial) and analyzed with our own code developed in R (R Core Team 2019).

The wavelength scale for the spectra was set using the dispersion per pixel and the distance of a pixel from the zero-order image. The dispersion for the SA-100 grating on the Rea 80-mm telescope was determined from spectra of planetary nebulae NGC 3132 and NGC 5315. The pixel-to-nanometer

Table 2. Target and comparison stars.

Star	*Spectral Class*	*T_{eff} (K)*[b]	*Variable Type*[a]	*Brightness Range (V mag)*[a]	*Period (days)*[a]	*C2 / C5*[c]	*Wing C3 / TiO*[c]	*Azizi C2 / TiO*[c]
R Oct	M5.3-M8.4e	2571	Mira	6.4–13.2	407	1.04 (0.43)	4.92 (0.94)	3.28 (0.57)
BQ Oct	M4III	3442	LB	6.80	—	3.36 (0.21)	2.21 (0.15)	2.05 (0.15)
CV Oct	M3	3507	LB	8.92–9.19	—	3.07 (0.39)	2.63 (0.37)	2.27 (0.25)
ε Oct	M5III	3355	SRB	4.58–5.30	55	—	4.08 (0.29)	2.81 (0.19)
CQ Oct	M4/M5III	3358	SRB	8.12–8.59	50.8	2.49 (0.20)	3.82 (0.30)	2.76 (0.19)
BW Oct	M5-M7III	2849	LB	7.90–9.10	—	1.12 (0.06)	5.85 (0.41)	3.26 (0.20)

[a] *The spectral type and variability data are taken from the AAVSO Variable Star Index (VSX). LB = slow irregular late type variables. SRB = Semi-regular type B, late type giants with poorly defined periodicity.*

[b] *The photospheric effective temperatures are taken from McDonald* et al. *(2012). R Oct is included in the McDonald* et al. *(2012) catalog under the identification HIP 25412.*

[c] *Average of ratios measured as described in section 2.2. Standard deviations given in brackets.*

conversion was averaged for the two lines (Hα and Hγ) and the two nebulae, giving a dispersion of 1.4880 nm/pixel. The OIII and Hβ lines were merged at this low resolution and were unsuitable for determining the per-pixel wavelength scale. This remained constant throughout the work as the distance between the filter wheel and the CCD was fixed.

The zero-point of a spectrum's wavelength scale is directly affected by uncertainty in the position of the center of the zero-order image for the star (often overexposed). The accuracy of the wavelength calibration is also affected by small changes in the alignment of the first order spectrum on the CCD chip (due to rotation of the grating in the filter holder) and higher order dispersion terms. These effects were sometimes noted in the spectrum but were estimated to cause systematic error no more than three pixels (less than 5 nm) at the key continuum point of 756 nm.

This level of uncertainty in wavelength scale is usual for low resolution spectra obtained through CCD imaging with filter wheel gratings. Our goal is to develop a diagnostic method which is accessible to non-professional astronomers and easily incorporated into existing and future crowd sourcing campaigns like those hosted by the AAVSO. To that end, we have consciously explored an approach which does not require accurate wavelength and/or flux calibration. The Wing (1992) filter system is our inspiration but we are *not* reproducing it by integrating the observed spectra over comparable band passes. Instead, our method relies on measuring the ratio between local flux peaks and troughs easily identified, even by visual inspection, near the central wavelengths of the Wing (1992) filters and the Kirkpatrick *et al.* (1991) quasi-continuum points. Reference to C1-C6 and the Wing A in our measurements refer to the flux of the peak or trough in the recorded flux found within about 7.5 nm of those wavelengths.

Figure 1 presents three spectra of R Oct from near maximum, mid, and minimum light with the continuum points from Table 1 marked. To minimize the impact on flux measurements from errors due to accuracy of the wavelength scale, the counts for each quasi-continuum point were measured at the local maximum within five pixels (≈ 7.5 nm) of their expected location. Each quasi-continuum point was visually inspected to verify that the pixel capturing the local maximum had been found. The depth of the TiO feature near 719 nm for the Wing A flux was determined in a similar manner using the flux from the pixel at the local *minimum*.

The signal-to-noise ratio (SNR) in the spectra decreased significantly as R Oct approached minimum brightness (see Figure 1). Both the decrease in SNR and the shifting of flux to longer wavelengths increase the uncertainty in the flux measured at the C1 quasi-continuum point and the bottom of the 719-nm TiO absorption line. Near minimum brightness, as many 16 to 25 individual images were stacked to create a spectrum with better SNR near minimum light. Despite best efforts, the influence of noise is more significant when the star is fainter than 12 magnitude. Worst case scenario, on the nights near minimum brightness with the highest sky background the SNR in the C1 and TiO measurements dipped as low as 3–4, translating into a 20–30 % error in ratios containing those measurements. Increased random noise is obvious in the ratios measured near minimum (see section 5).

Figure 2 illustrates how low spectral resolution and the growth of absorption features in later/cooler spectral types influence the measurement of the spectra. The Wing and Azizi ratios rely on the growth of the TiO absorption feature near 719 nm relative to the continuum. The overall shape of the spectra are influenced by the underlying blackbody continuum as it changes with the star's effective temperature.

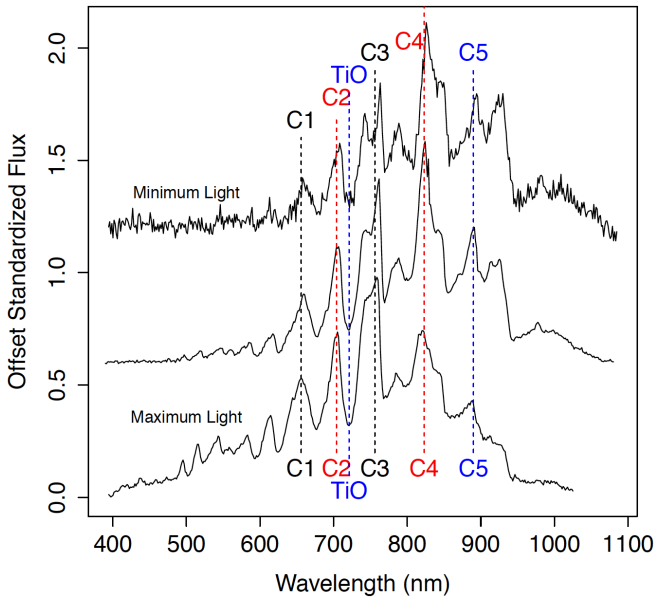

Figure 1. Spectra of R Oct at three epochs between maximum and minimum light. The quasi-continuum points C1 through C5 of Table 1 plus the TiO absorption line at 719 nm used by both the Wing A/C3 and Azizi A/C2 ratio have been labeled. Note that Wing B and C3 and the continuum point used by Aziz and C2 are equivalent as measured using the method employed at low spectral resolution.

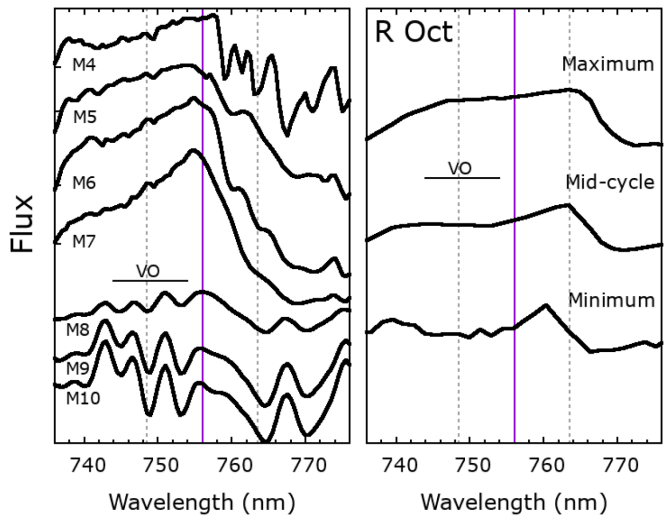

Figure 2. The left panel shows representative M type giant (luminosity class III) spectra from the Pickles (1998) spectral library covering the usual temperature range of R Oct. The right panel shows the low resolution spectra observed for R Oct at maximum brightness/hottest (2017 Feb 20), mid-cycle (2017 June 26), minimum brightness/coolest (2017 Sep 16). The position is marked for the VO absorption features which influence the measurement of C3 at later/cooler spectral types. The solid vertical line is the location of the C3, the quasi-continuum point, and the dotted vertical lines mark the ± 7.5-nm range on either side used to find the local maximum.

As reported by Azizi and Mirtorabi (2015), both the library spectra and the spectra of the target reveal the influence of VO absorption on the C3 quasi-continuum point at spectral types M8 and later. Low spectral resolution "blurs" nearby absorption features so that *none* of the Kirkpatrick *et al.* (1991) continuum points are free of absorption influence in the spectra recorded for this project. But Figure 2 shows that our method of using the local maximum to measure the low resolution spectra of R Oct best samples the quasi-continuum that is present.

In addition to changing absorption bands, Mira variables also undergo large swings in effective temperature that significantly affect the flux distribution of the spectrum over their cycle. When R Oct is spectral type M4-M5 near maximum brightness the spectrum clearly shifts toward blue/shorter wavelengths (Figure 1). When measuring the earliest spectral types (M1-M5) it is difficult to identify a local maximum to measure the flux of longest wavelength quasi-continuum points (C4 to C6). This is why the Wing and Azizi ratios, primarily developed for early spectral types, focus on the shorter wavelength end of the spectrum. Since R Oct gets much cooler than M5, focus must to shift to longer wavelengths to measure its temperature changes. A significant drop in quantum efficiency of silicon based CCD detectors at longer wavelengths also contributes to difficulty measuring flux at C4-C6 (see section 3.2).

3. Ratios from continuum points

3.1. Continuum ratios from library spectra

While the presence and strength of key absoprtion features is considered the best way to measure the spectral type, the continuum points identified by Kirkpatrick *et al.* (1991) (Table 1) should also be influenced by change in blackbody temperature. The curves plotted in Figure 3 illustrate that across spectra types M0 to M10 there is a steady change in the ratio of the flux between continuum points corresponding to the effective temperature.

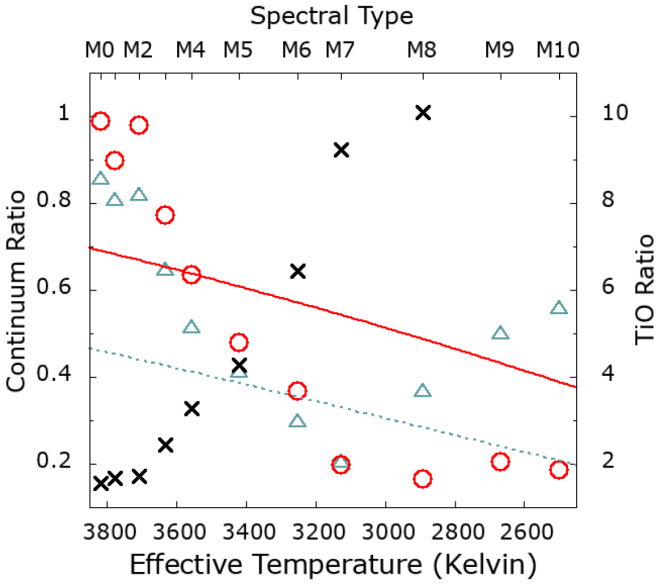

Figure 3. Ratios of the continuum points C1/C3 (triangles), C2/C5 (circles), and Wing C3/TiO ratio (X's, right y-axis) computed from library spectra (Pickles 1998) over a range of spectral types. The dashed line is the C1/C3 ratio from a pure blackbody. The solid line is the C2/C5 ratio from a pure blackbody. The quasi-continuum ratios are read off the y-axis on the left and the Wing ratio is read off the axis on the right. The ratios plotted only account for the relative flux in the library spectra and from the blackbody function. They do not account for the sensitivity of the CCD.

The flux at the Kirkpatrick *et al.* (1991) continuum points was measured in the library spectra of giants (luminosity class III) published by Pickles (1998). To reproduce what was done with the observed spectra, fluxes in the library spectra were recorded at the local maximum within ± 7.5 nm of each continuum point. The Wing TiO absorption (Wing A filter) was measured as the local minimum within ± 7.5 nm of 719 nm. The continuum point C6 was excluded from this analysis because the sensitivity of most CCDs are very low (quantum efficiency < 20%) at wavelengths greater than 900 nm.

Of the ratios investigated, the C2/C5 and C1/C3 ratios show the most pronounced and clear variation across the M spectral types for giants. As expected, the ratios measured from the Pickles (1998) library spectra differ significantly from those predicted for a pure blackbody (Figure 3). This demonstrates how the absorption features influence the "continuum" points at low spectral resolution. Careful investigation of the template spectra within 10 nm of C1 and C2 show that the general appearance of the spectrum around those points is relatively similar across all M spectral types. However within 10 nm of C3 and C5 the shape of the spectrum changes substantially by adding several significant absorption features in spectral types M9 and cooler. Regardless, each continuum point still shows a clear dependence on spectral type whether they are free from the influence of absorption or not.

As shown in previous work (Rea 2019), the Wing TiO/C3 ratio, measuring the relative depth of the 719 nm TiO absorption feature, is a reliable indicator of effective temperature in low resolution spectra of earlier spectral types. When measuring the flux at the local maximum, Wing (1992) B is equivalent to C3. The Wing TiO/C3 ratio shows clear variation in the earlier spectral types (M0-M5). In later spectra types (M6-M10) the TiO absorption near 719 nm becomes saturated and the depth of the band cannot be distinguished from a flux of zero in observed spectra.

Of the continuum ratios investigated, C2/C5 shows the most variation, decreasing in value by a factor of almost 9 between spectral types M2 and M8 (Figure 3). This behavior is comparable to performance of Wing (1992) C3/A ratio but with a steeper slope with respect to effective temperature and no limiting factor like the TiO band saturating. As a result, we predict that C2/C5 shows promise as a temperature indicator in the middle of the M spectral types. That makes it well suited to measure the effective temperature change of R Oct which varies between spectral types M5-M8. However, note that while the C2/C5 ratio shows promise in the mid-range of spectral types, it shows no significant variation in earliest (M0-M2) and latest spectra types (M8-M10).

Neither the C2/C5 or Wing (1992) C3/A ratio are sensitive to changes in temperature in the latest spectral types (M8-M10). This presents a problem for measuring variation in the coolest Mira variables. Fortunately, the C1/C3 ratio is predicted to show variation through latest spectral types (M7-M10). The trend of that ratio reverses near M7 so there is aliasing

of ratio values between late and early spectral types. In future work, that aliasing could be disentangled using other indicators to create a two dimensional index (i.e. brightness of star near minimum/coolest, Wing C3/A, or C2/C5).

3.2. Practical considerations

The approach used in this work to measure the spectra of R Oct is appealing for low resolution slit-less spectroscopy because it does *not* require accurate wavelength calibration of the spectra. Using the local maximum or minimum to measure the flux allows the method to be applied even via visual inspection.

The ratios calculated in Figure 3 do *not* include consideration of CCD efficiency or flat fielding effects on the extracted spectrum. The CCD sensitivity as a function of wavelength acts like a multiplicative factor for all ratios. Note that C1 is near the peak sensitivity of most CCDs. The Sony ICX424AL CCD used in this study has a bluer response peaking closer to 500 nm. The solid state physics of silicon dictates that the sensitivity of most CCDs decreases by more than a factor of two between C2 and C5 and they are less than 20% efficient at wavelengths longer than 900 nm. The sensitivity of most silicon detectors is much too low to effectively measure the flux of C6.

As noted in section 2.3, at low spectral resolution (R ~ 100) it becomes very difficult to accurately measure C4, C5, and C6 in early spectral types. In M3 and earlier spectral types the molecular absorption around C4-C6 decreases in strength and it is harder to distinguish absorption from continuum. That, combined with low spectral resolution, obliterates the spectral "peak" near those points and makes it difficult to accurately employ the our method to measure the spectral flux without accurate wavelength calibration.

Flat fielding effects in the images and sampling at different spectral resolutions could also influence the continuum ratios. *This implies that it is important to calibrate each telescope, grating, and camera combination with comparison stars of known spectral type.* A selection of comparison stars with spectral types covering the range of the target's pulsation should be used to calibrate the relationship between ratio value and spectral type for a given equipment setup. To avoid changes in the observed ratios due to flat fielding effects, the spectrum should always be recorded in the same part of the field. And for the highest accuracy, the sky background/illumination (i.e. the Moon, during dusk) should be monitored and subtracted from the extracted spectrum.

4. Results

4.1. The comparison stars

Spectra of five comparison stars observed between April and September 2018 were used to calibrate the spectral ratios recorded for R Oct with the Rea 80 mm telescope. Those spectra are similar to those recorded for R Oct and described in detail in Rea (2019). That work showed only BW Oct and CQ Oct exhibited any significant change in brightness over the period of observation.

The method used to measure the R Oct spectrum was also used to measure the continuum fluxes for each comparison star spectrum. The average and standard deviation of the C1/C3, C2/C5, Wing C3/TiO, and Azizi C2/TiO ratios are given in Table 2 and the results for the C2/C5 ratio are plotted as a function of photospheric effective temperature in Figure 4.

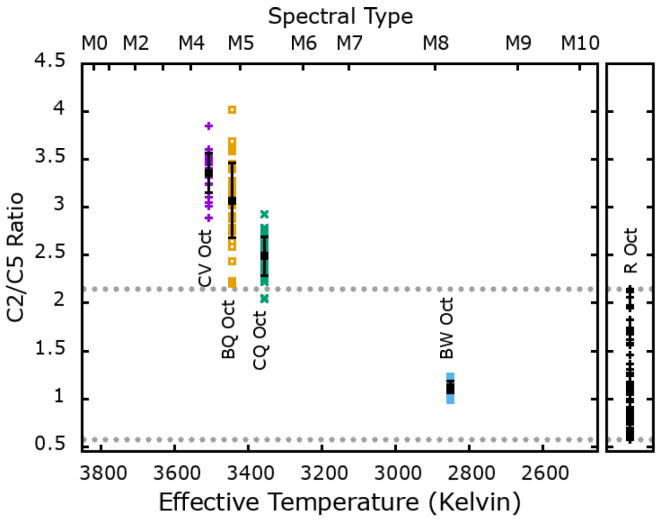

Figure 4. A plot of the C2/C5 ratio measured from the spectra of the comparison stars plotted against their surface temperature. Horizontal dotted lines mark the minimum and maximum C2/C5 ratio measured for R Oct. The distribution of ratio values measured for R Oct are shown on the right on the same y-scale in the detached panel.

Only CV Oct shows any evidence of a change in its spectral ratios over that period. The average C1/C3 and C2/C5 ratios for CV Oct were slightly lower in the first half relative to the second half of the period of observation, but not significantly so.

4.2. Results from R Oct

The period along with the range of spectral type and brightness of Mira variable R Oct are given in Table 2. In addition to being a cooler Mira variable, R Oct is desirable as a target because it is near the south celestial pole and can be observed year round from New Zealand. No part of the cycle was lost due to solar conjunction.

The 80-mm Rea telescope was used to collect 93 spectra of R Oct between 11 October 2015 and 25 September 2018, an interval that covered approximately two and a half pulsation cycles. The Bright Star Monitor South measured its brightness in Johnson B and V starting 12 November 2017. When the B magnitude dropped below about 13, the I filter was used in place of B. All the photometry obtained for this study are available for download from the AAVSO International Database (https://www.aavso.org/data-download) submitted by observer RWSA (William Rea). Prior to November 2017, the brightness of R Oct is tracked using the visual estimates of Ejii Kato (observer ID KEI) submitted to the AAVSO International Database. While there are other visual estimates for R Oct in the AAVSO International Database, we relied exclusively on Kato's observations since they were made by a single reliable observer (no concern of differences between observers) and covered the same epochs as the spectra recorded for R Oct.

Spectra were extracted and measured as outlined in section 2.3. Figure 6 shows the Wing TiO/C3 and Aziz TiO/C2

Table 3. Observed Brightness and Spectral Ratios for R Oct.

JD –2450000	Visual Mag[a]	V_{mag}	(B–V)	C1/C3	C2/C5	Wing A/B	Azizi
7306	—	—	—	0.36	0.89	4.49	2.82
7313	—	—	—	0.35	0.90	4.84	2.95
7315	10.4	—	—	0.38	0.81	4.46	2.65
7331	—	—	—	0.36	0.98	4.19	2.56
7339	—	—	—	0.34	0.97	4.67	2.87
7345	9.9	—	—	—	—	—	—
7347	—	—	—	0.37	1.13	4.52	2.70
7358	—	—	—	0.36	1.05	4.65	2.72
7370	—	—	—	0.48	1.71	4.31	3.21
7371	8.8	—	—	—	—	—	—
7381	—	—	—	0.56	1.98	3.59	2.72
7391	—	—	—	0.54	2.12	3.18	2.42
7396	—	—	—	0.58	2.15	3.16	2.47
7405	7.7	—	—	—	—	—	—
7407	—	—	—	0.59	2.06	3.30	2.55
7419	—	—	—	0.57	1.83	2.99	2.16
7427	8.4	—	—	—	—	—	—
7436	8.8	—	—	—	—	—	—
7441	—	—	—	0.46	1.46	4.03	2.65
7450	—	—	—	0.42	1.24	4.57	2.85
7457	—	—	—	0.46	1.31	4.50	2.99
7474	—	—	—	0.36	1.12	5.23	3.15
7479	9.9	—	—	—	—	—	—
7483	—	—	—	0.40	1.24	5.19	3.57
7488	—	—	—	0.34	1.27	5.84	3.37
7492	10.3	—	—	—	—	—	—
7502	10.4	—	—	—	—	—	—
7503	—	—	—	0.34	0.88	5.36	3.01
7515	—	—	—	0.31	0.82	5.70	3.14
7520	11.2	—	—	—	—	—	—
7526	—	—	—	0.40	0.90	5.99	3.86
7534	11.4	—	—	—	—	—	—
7533	—	—	—	0.34	0.77	5.52	3.34
7541	—	—	—	0.33	0.68	4.92	3.00
7548	11.6	—	—	—	—	—	—
7565	12.2	—	—	—	—	—	—
7570	—	—	—	0.40	0.63	5.73	3.30
7578	12.5	—	—	—	—	—	—
7581	—	—	—	0.35	0.63	5.47	3.55
7590	—	—	—	0.21	0.68	5.33	3.60
7599	12.9	—	—	—	—	—	—
7607	—	—	—	0.21	0.57	8.01	4.82
7622	—	—	—	0.34	0.64	4.77	2.99
7628	12.8	—	—	—	—	—	—
7629	—	—	—	0.40	0.60	4.89	3.10
7634	—	—	—	0.37	0.64	6.34	3.95
7651	12.5	—	—	—	—	—	—
7648	—	—	—	0.38	0.66	4.61	3.14
7666	—	—	—	0.41	0.73	4.77	3.45
7673	—	—	—	0.34	0.70	5.01	3.11
7680	12.2	—	—	0.34	0.65	3.61	2.18
7691	—	—	—	0.38	0.73	5.12	3.35
7697	11.6	—	—	—	—	—	—
7699	—	—	—	0.29	0.62	4.30	2.54
7703	11.2	—	—	—	—	—	—
7711	—	—	—	0.35	0.78	4.93	3.11
7719	—	—	—	0.35	0.78	4.84	3.21
7736	10.4	—	—	—	—	—	—
7741	—	—	—	0.49	1.13	4.14	3.18
7754	—	—	—	0.44	1.18	4.07	2.70
7758	9.4	—	—	—	—	—	—
7763	9.2	—	—	—	—	—	—
7765	—	—	—	0.51	1.58	3.74	2.79
7776	—	—	—	0.54	1.62	3.24	2.40
7777	8.7	—	—	—	—	—	—
7786	—	—	—	0.54	1.69	3.02	2.24
7790	8.3	—	—	—	—	—	—
7793	—	—	—	0.54	1.73	3.32	2.51
7804	—	—	—	0.54	1.73	3.75	2.72
7807	8.4	—	—	—	—	—	—
7815	—	—	—	0.50	1.67	3.84	2.67
7828	—	—	—	0.48	1.74	4.33	3.04
7829	8.4	—	—	—	—	—	—
7839	8.8	—	—	—	—	—	—
7850	8.9	—	—	—	—	—	—
7852	—	—	—	0.37	1.15	4.76	2.83
7858	—	—	—	0.41	1.27	5.43	3.44
7859	9.4	—	—	—	—	—	—
7865	—	—	—	0.37	1.17	5.53	3.35
7873	10.0	—	—	—	—	—	—
7874	—	—	—	0.38	1.10	5.81	3.56
7886	—	—	—	0.39	1.05	5.12	3.26
7890	10.5	—	—	—	—	—	—
7904	10.8	—	—	—	—	—	—
7920	11.1	—	—	—	—	—	—
7930	—	—	—	0.39	0.87	5.31	3.50
7935	11.6	—	—	—	—	—	—
7952	—	—	—	0.48	0.81	4.29	3.29
7955	11.9	—	—	—	—	—	—
7959	—	—	—	0.37	0.69	5.22	3.20
7966	12.4	—	—	—	—	—	—
7970	—	—	—	0.38	0.79	5.62	3.46
7977	12.5	—	—	—	—	—	—
7983	—	—	—	0.39	0.62	4.59	2.90
7989	—	—	—	0.34	0.59	4.44	2.95
7994	12.9	—	—	—	—	—	—
8000	—	—	—	0.35	0.67	5.82	4.56
8007	13.0	—	—	—	—	—	—
8012	—	—	—	0.43	0.60	5.51	3.93
8019	12.9	—	—	—	—	—	—
8026	—	—	—	0.36	0.58	4.94	3.80
8036	12.9	—	—	—	—	—	—
8038	—	—	—	0.42	0.90	5.11	3.84
8045	—	—	—	0.38	0.61	6.48	3.60
8056	12.8	—	—	0.32	0.62	6.33	3.84
8068	—	—	—	0.40	0.63	4.73	2.98
8069	12.4	—	—	—	—	—	—
8070	—	11.992 ± 0.038	—	—	—	—	—
8071	—	11.944 ± 0.063	2.06	—	—	—	—
8072	—	11.907 ± 0.036	—	—	—	—	—
8076	—	11.901 ± 0.048	—	—	—	—	—
8078	—	11.792 ± 0.043	—	—	—	—	—
8079	—	11.823 ± 0.044	1.885	0.35	0.63	5.04	3.23
8082	12.2	—	—	—	—	—	—
8089	—	11.615 ± 0.052	—	0.38	0.70	5.07	3.31
8093	11.9	—	—	—	—	—	—
8094	—	11.471 ± 0.043	—	—	—	—	—
8096	—	11.504 ± 0.045	2.01	—	—	—	—
8100	—	11.349 ± 0.045	2.14	—	—	—	—
8102	11.6	11.298 ± 0.064	1.986	—	—	—	—
8103	—	11.314 ± 0.027	1.699	0.29	0.61	4.68	2.72
8109	—	11.134 ± 0.024	1.981	—	—	—	—
8113	—	11.108 ± 0.039	1.85	—	—	—	—
8114	—	11.111 ± 0.032	1.812	—	—	—	—
8118	—	10.965 ± 0.04	1.198	—	—	—	—
8120	—	11.021 ± 0.056	1.25	—	—	—	—
8122	—	11.058 ± 0.039	1.775	—	—	—	—
8123	—	11.007 ± 0.05	1.777	—	—	—	—
8124	11.4	—	—	—	—	—	—
8128	—	10.958 ± 0.044	1.709	—	—	—	—
8132	—	—	—	0.45	0.86	4.82	3.63
8134	—	10.851 ± 0.032	1.75	—	—	—	—

Table continued on next page

Table 3. Observed Brightness and Spectral Ratios for R Oct, cont.

JD –2450000	Visual Mag[a]	V_{mag}	(B–V)	C1/C3	C2/C5	Wing A/B	Azizi	JD –2450000	Visual Mag[a]	V_{mag}	(B–V)	C1/C3	C2/C5	Wing A/B	Azizi
8135	—	10.812 ± 0.027	1.641	—	—	—	—	8275	10.2	—	—	—	—	—	—
8137	—	10.767 ± 0.056	1.642	—	—	—	—	8277	—	—	—	0.34	0.99	6.09	3.61
8146	—	—	—	0.41	0.86	5.36	3.46	8280	—	10.001 ± 0.021	1.621	—	—	—	—
8147	—	10.767 ± 0.056	1.642	—	—	—	—	8288	10.5	—	—	—	—	—	—
8154	—	10.527 ± 0.053	1.698	—	—	—	—	8289	—	10.277 ± 0.031	1.521	—	—	—	—
8155	11.1	—	—	—	—	—	—	8291	—	—	—	0.32	0.83	5.43	3.29
8156	—	—	—	0.39	0.86	5.45	3.38	8301	—	10.673 ± 0.041	1.491	—	—	—	—
8166	—	—	—	0.44	1.09	4.96	3.38	8302	—	—	—	0.38	0.85	6.28	3.95
8180	—	—	—	0.48	1.36	4.53	3.13	8310	10.8	—	—	—	—	—	—
8189	8.7	—	—	—	—	—	—	8311	—	—	—	0.35	0.86	6.96	4.43
8191	—	8.314 ± 0.049	1.425	—	—	—	—	8320	11.5	—	—	—	—	—	—
8195	—	—	—	0.52	1.94	4.06	3.05	8321	—	—	—	0.43	0.92	6.65	4.50
8200	—	7.787 ± 0.046	1.473	—	—	—	—	8322	—	11.149 ± 0.031	1.732	—	—	—	—
8203	8.3	—	—	—	—	—	—	8332	—	11.342 ± 0.034	—	—	—	—	—
8206	—	7.664 ± 0.039	1.499	0.51	1.96	4.03	2.85	8333	—	—	—	0.44	0.81	5.75	4.06
8212	—	7.652 ± 0.045	1.456	—	—	—	—	8336	—	11.393 ± 0.047	—	—	—	—	—
8217	8.2	—	—	—	—	—	—	8340	—	11.512 ± 0.028	—	—	—	—	—
8224	8.3	—	—	0.50	1.82	4.16	3.03	8341	—	—	—	0.39	0.83	5.09	3.50
8227	—	7.962 ± 0.031	1.528	—	—	—	—	8345	—	11.668 ± 0.02	—	—	—	—	—
8231	—	8.061 ± 0.047	1.543	—	—	—	—	8342	12.0	—	—	—	—	—	—
8233	—	—	—	0.42	1.56	4.68	3.07	8349	—	—	—	0.44	0.89	5.39	4.06
8236	8.7	—	—	—	—	—	—	8351	12.4	—	—	—	—	—	—
8239	—	8.327 ± 0.018	1.539	—	—	—	—	8356	—	—	—	0.50	0.83	6.11	4.74
8252	—	8.838 ± 0.033	1.515	—	—	—	—	8365	—	12.066 ± 0.045	—	—	—	—	—
8255	—	—	—	0.39	1.15	4.74	2.89	8368	—	—	—	0.38	0.76	5.78	3.83
8257	—	—	—	0.39	1.11	4.63	2.80	8373	—	12.261 ± 0.041	—	—	—	—	—
8259	9.5	—	—	—	—	—	—	8375	—	—	—	0.42	0.68	7.19	4.70
8264	—	9.327 ± 0.019	1.575	—	—	—	—	8381	—	12.464 ± 0.037	—	—	—	—	—
8268	—	9.52 ± 0.024	1.511	—	—	—	—	8386	—	—	—	0.45	0.69	4.48	3.40
8272	—	9.727 ± 0.051	1.51	—	—	—	—								

[a] *By Eiji Kato (Observer ID: KEI) from the AAVSO International Database (Kafka 2020).*

ratios and Figure 7 shows the C2/C5 and C1/C3 ratio measured compared with the fluctuating brightness of the target. The data in those Figures are given in Table 3.

5. Discussion

Figure 5 presents more than a century's worth of visual and, later, Johnson V band observations of R Oct. Taking only the visual observations, the brightness has ranged over eight magnitudes from 6 to 14. Note that the maxima and minima of the main 405.5-day period vary in brightness. Within any particular cycle the brightness range was typically between five and six magnitudes. These variations are sufficiently irregular that no longer term periods have been conclusively identified. Note in Figure 7 that the maximum brightness and shape of the brightness peak around each maximum varied significantly over the 2.5 cycles observed in this study but were towards the lower end of the historical range. Any spectral index that successfully measured R Oct should also capture these variations.

The Wing C3/TiO and Azizi C2/TiO ratios do not capture most of the variation in R Oct's cycle (see Figure 6). When the R Oct is hottest, near the peak of its brightness, there is some noticeable decrease in both ratios (more in Wing than in Azizi) but the remainder of the cycle both are mostly the same unvarying value. The abrupt increase ("spikes") in both observed ratios near minimum brightness are caused by the spectrum becoming faint and noisy and the depth of the TiO absorption increasing so that it approaches the zero level in the spectrum (see section 2.3).

The failure of the Wing ratio in late spectral types was expected and primarily attributed to the increase in VO absorption near C3. Azizi and Mirtorabi (2015) formulated their ratio with the intention of applying it to higher resolution spectra. Rea (2019) and this result demonstrate that the Azizi ratio is not as sensitive as the Wing ratio when using low spectral resolution.

The C2/C5 ratio followed changes in R Oct throughout the 2.5 cycles observed (Figure 7). The range of values of the C2/C5 ratio is compared to the ranges of the comparison stars in Figure 4). That Figure confirms other authorities who give R Oct's spectral type as about M5.5 at maximum light. At minimum light the C2/C5 ratio is much lower that the closest comparison star, BW Oct, which has a published spectral classification of M7.

Other ratios (C1/C4, C2/C4, and C1/C5, Figure 8) show results that are similar to C2/C5. However, C2/C5 is favored because it has the steepest predicted slope with respect to spectral type and the measurements of C2/C5 from the spectra of R Oct have a larger range of values than the other ratios. Ratios using C1 are less desirable because C1 is fainter and more uncertain due to increased noise in R Oct's spectrum near minimum brightness (section 2.3).

The differences in the three peaks of the light curve around maximum brightness (i.e. change in peak brightness, and shape

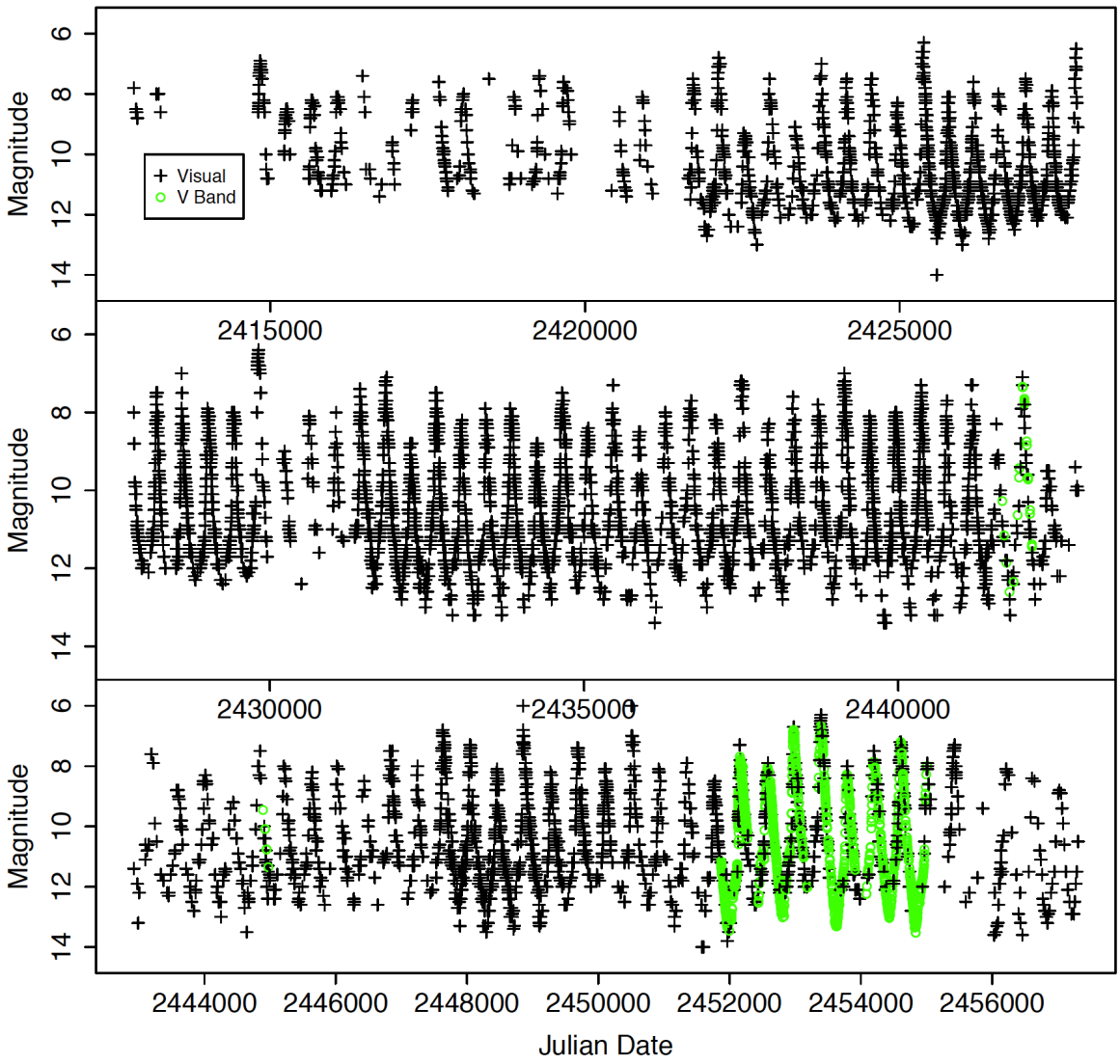

Figure 5. The visual (black) and V band (green) observations of R Oct in the AAVSO International Database up until the start of the study period. The visual estimates of the magnitude range from 6 to 14.

of light curve) are tracked closely by the C2/C5 ratio. The C2/C5 ratio clearly reveals that R Oct's surface was hotter when the maximum was brighter and that it stayed hotter longer when the maximum was broad instead of sharply peaked. It is not clear from this data if R Oct was always roughly the same spectral type at minimum brightness or if C2/C5, as predicted, becomes insensitive to changes around spectral type M7 or M8. Correlating R Oct's C2/C5 ratio with the comparison stars in Figure 4 reveals that at peak brightness R Oct had a spectral type that was similar to CQ Oct (spectral type M 5.5) and at minimum it was later in spectral type than BW Oct (spectral type M7).

Analysis in section 3 predicts that the C1/C3 ratio should be sensitive to changes in M type giants later than spectral type M7. R Oct is supposed to get as late as spectral type M8.4 (deLaverny *et al.* 1997) and comparison of R Oct's C2/C5 ratio with BW Oct implies that over the period of this study R Oct got later than M7. The C2/C3 and C1/C2 ratios are also predicted to react to changes in late spectral types in a manner similar to C1/C3. However, in R Oct's spectrum only C1/C3 showed significant correlation with the changing brightness of the star. We conclude that the spacing between adjacent continuum points is too small to be sensitive to temperature changes in these low resolution spectra.

Aside from some variation near peak brightness, Figure 7 shows no significant variation in the C1/C3 ratios measured for R Oct over 2.5 cycles. This does not support the prediction made in section 3 that the C1/C3 ratio should "rebound" and increase as R Oct reached its latest spectral type near minimum. Instead the C1/C3 variation flattens and becomes more random when R Oct's brightness dips fainter. The noise level in the spectrum only contributes significantly when R Oct gets fainter than 12.0 (section 2.3). However, note that the C1/C3 ratio flattens *before* the star's brightness drops fainter than 10.0; at about the same point the Wing ratio also loses sensitivity. Therefore we cannot exclude that this effect is influenced by additional factors like absorption features filtered through the "blurring" influence of low spectra resolution. The observational limitations of our study prevent us from reaching a clear conclusion.

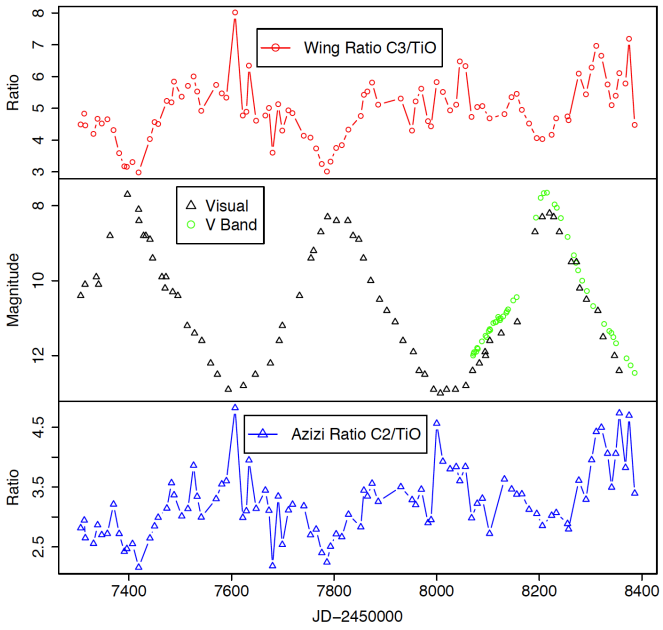

Figure 6. Wing C3 / TiO (top panel) and Azizi C2 / TiO (bottom panel) measured from spectra, and the brightness of R Oct (middle panel) over about 2.5 cycles between 11 October 2015 and 25 September 2018.

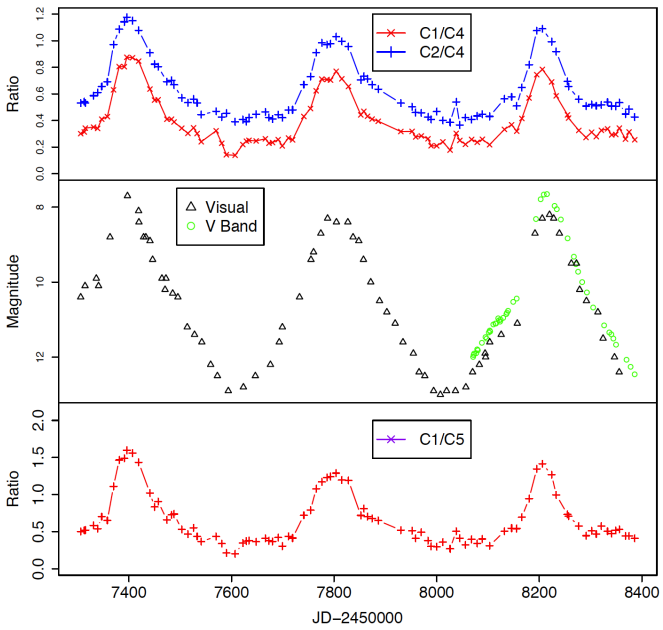

Figure 8. The C1/C4 and C2/C4 ratios (top panel) and C1/C5 ratio (bottom panel) measured from spectra, and the brightness of R Oct (middle panel) over about 2.5 cycles between 11 October 2015 and 25 September 2018.

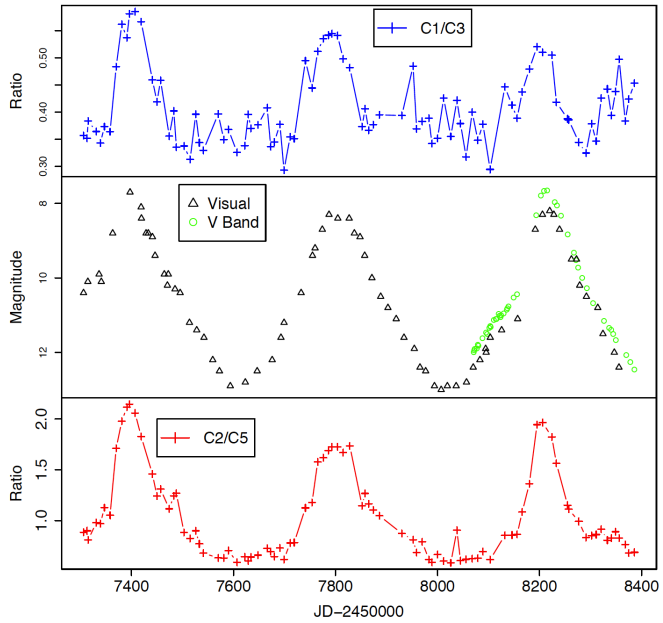

Figure 7. The C1/C3 (top panel) and C2/C5 (bottom panel) ratios measured from spectra, and the brightness of R Oct (middle panel) over about 2.5 cycles between 11 October 2015 and 25 September 2018.

6. Conclusions and future directions

R Oct and other circumpolar Miras offer excellent opportunities to include grating spectroscopy in a CCD photometric observing program. Low resolution spectral observations add scientific value beyond what can be obtained from multi-color photometry. For Miras with very long histories of visual observation, low resolution spectroscopy adds to understanding of these "legacy" stars. To maximize their contribution observers must be well aware of how to use comparison stars to calibrate their observing setup and understand how noise limits their measurements.

The measure of TiO absorption strength, which we refer to as the Wing and Azizi ratios, is ineffective for measuring the physical changes of R Oct around its cycle since its spectral type is always later than M5. The linear response of CCD chips compared to photographic emulsions allows us to transition from relying on absorption line strength and appearance to determining spectral type from continuum points that sample the shape of the underlying blackbody curve. In late type stars, spectroscopy offers an advantage over even narrow band photometry in the ability to more finely select quasi-continuum points and measure their flux, even without highly accurate wavelength calibration. The C1 / C3 ratio and the C2 / C5 ratios are the two most reliable guides to R Oct's changes in effective temperature over the course of its pulsation cycle. The C2 / C5 ratio is sensitive to all the fine details in the visible light curve around peak brightness. However, both C2 / C5 and C1 / C3 appear to become less sensitive to changes in spectral type as R Oct approaches minimum brightness, due at least in part to increased noise when R Oct was fainter than 12th magnitude. However, it is unclear if other factors may contribute.

This work is limited by having only one cool comparison star and no comparison stars cooler than spectral type M7. It is unclear if R Oct was the same temperature at each minimum or if the C2 / C5 ratio is insensitive to change below spectral type M7. Having more comparison stars and more cool comparison stars over the full expected range of the target could yield more precise results. Future work should explore if there is a low temperature failure point of C2 / C5 ratio and if C1 / C3 is sensitive to change in the coolest M type giants. However, we acknowledge that work will face significant challenges when identifying suitable M-type comparison giants of the latest types since they are rare and tend to be variable.

7. Acknowledgements

We thank Robert Wing for the email discussions about his three- and eight-filter photometry systems and the particular problems posed by the presence of the VO molecule in the coolest Miras. We thank Arne Henden, Michael Nicholas, George Silvis, and Bill Toomey of the AAVSO for their help in operating the AAVSO's Bright Star Monitor telescopes. We thank Tim Crawford of the AAVSO comparison star team for adding further suitable comparison stars to fields captured by the BSM telescopes used in this project. We thank the AAVSO observers who contributed to the observations AAVSO's International Database used in this study. Without the assistance and encouragement of these people this study would not have been possible.

References

Azizi, F., and Mirtorabi, M. T. 2015, *Astrophys. Space Sci.*, **357**, 96.

Benn, D. 2012, *J. Amer. Assoc. Var. Star Obs.*, **40**, 852.

Celis, S. L. 1978, *Astron. Astrophys.*, **63**, 53.

de Laverny, P., Geoffray, H., Jorda, L., and Kopp, M. 1997, *Astron. Astrophys., Suppl. Ser.*, **122**, 415.

Gray, R. O., and Corbally, C. J. 2009, *Stellar Spectral Classification*, Princeton University Press, Princeton, NJ.

Kafka, S. 2020, variable star observations from the AAVSO International Database (https://www.aavso.org/aavso-international-database-aid).

Keenan, P. C. 1966, *Astrophys. J., Suppl. Ser.*, **13**, 333.

Kirkpatrick, J. D., Henry, T. J, and McCarthy, D. W. 1991, *Astrophys. J., Suppl. Ser.*, **77**, 417.

Martin, J. C., Rea, B., McFarland, R., and Templeton, M. 2016a, 2016 Symposium Videos (http://socastrosci.org/Video2016.html), Society for Astronomical Sciences, Rancho Cucamonga, CA.

Martin, J. C., Rea, B., McFarland, R., and Templeton, M. 2016b, SAS Publications (http://socastrosci.org/Publications.html), Society for Astronomical Sciences, Rancho Cucamonga, CA.

Mattei, J. A. 1997, *J. Amer. Assoc. Var. Star Obs.*, **25**, 57.

McDonald, I., Zijlstra, A. A., and Boyer, M. L. 2012, *Mon. Not. Roy. Astron. Soc.*, **427**, 343.

Pickles, A. J. 1998, *Publ. Astron. Soc. Pacific*, **110**, 863.

R Core Team. 2019, R: A Language and Environment for Statistical Computing, R Foundation for Statistical Computing, Vienna, Austria (https://www.R-project.org).

Rea, B. 2019, *J. Amer. Assoc. Var. Star Obs.*, **47**, 70.

Serkowski, K., and Shawl, S. J. 2001, *Astron. J.*, **122**, 2017.

Wing, R. F. 1992, *J. Amer. Assoc. Var. Star Obs.*, **21**, 42.

Wing, R. F. 1997, *J. Amer. Assoc. Var. Star Obs.*, **25**, 63.

Zima, W. 2008, *Commun. Asteroseismology*, **155**, 17.